HHS Public Access

Author manuscript

J Mol Biol. Author manuscript; available in PMC 2023 January 30.

Published in final edited form as:

J Mol Biol. 2022 January 30; 434(2): 167400. doi:10.1016/j.jmb.2021.167400.

A model for the signal initiation complex between Arrestin-3 and the Src family kinase Fgr

Ivette Perez[1,3], **Sandra Berndt**[2,3], **Rupesh Agarwal**[4,5], **Manuel A. Castro**[1,3], **Sergey A. Vishnivetskiy**[2], **Jeremy C. Smith**[4,5], **Charles R. Sanders**[1,3], **Vsevolod V. Gurevich**[2], **T.M. Iverson**[1,2,3,6]

[1]Department of Biochemistry, Vanderbilt University, Nashville, TN 37232-0146;

[2]Department of Pharmacology, Vanderbilt University, Nashville, TN 37232-0146;

[3]Center for Structural Biology, Nashville, TN 37232-0146;

[4]Department of Biochemistry and Cellular and Molecular Biology, University of Tennessee, Knoxville, TN 37996;

[5]UT/ORNL Center for Molecular Biophysics, Oak Ridge National Laboratory, TN;

[6]Vanderbilt Institute of Chemical Biology, Nashville, TN 37232-0146;

Abstract

Arrestins regulate a wide range of signaling events, most notably when bound to active G protein-coupled receptors (GPCRs). Among the known effectors recruited by GPCR-bound arrestins are Src family kinases, which regulate cellular growth and proliferation. Here, we focus on arrestin-3 interactions with Fgr kinase, a member of the Src family. Previous reports demonstrated that Fgr exhibits high constitutive activity, but can be further activated by both arrestin-dependent and arrestin-independent pathways. We report that arrestin-3 modulates Fgr activity with a hallmark

To whom correspondence should be addressed: T.M. Iverson, Department of Pharmacology, Vanderbilt University, Nashville, TN 37232, USA, Telephone: 615-322-7817; tina.iverson@vanderbilt.edu; Vsevolod V. Gurevich, Department of Pharmacology, Vanderbilt University, Nashville, TN 37232, USA, Telephone: 615-322-7070; FAX: 615-343-6532; vsevolod.gurevich@vanderbilt.edu.

ACCESSION NUMBERS:
PDB: 7JT9

[1]We use systematic names of arrestin proteins, where the number after the dash indicates the order of cloning: arrestin-1 (historic names S-antigen, 48 kDa protein, visual or rod arrestin), arrestin-2 (β-arrestin or β-arrestin1), arrestin-3 (β-arrestin2 or hTHY-ARRX), and arrestin-4 (cone or X-arrestin).

CRediT author statement

Ivette Perez: Conceptualization, Methodology, Investigation, Formal Analysis, Validation, Writing. **Sandra Berndt** Conceptualization, Methodology, Investigation, Writing. **Rupesh Agarwal**: Software, Formal Analysis, Writing. **Manuel Castro**: Methodology, Investigation, Formal Analysis, Validation, Writing. **Sergey Vishnivetskiy**: Methodology, Investigation, Writing. **Jeremy Smith**: Supervision, Writing. **Charles Sanders**: Supervision, Writing. **Vsevolod Gurevich**: Conceptualization, Methodology, Supervision, Writing, Project management, Funding acquisition. **Tina Iverson**: Conceptualization, Methodology, Supervision, Writing, Project management, Funding acquisition.

Declaration of interests

The authors declare that they have no known competing financial interests or personal relationships that could have appeared to influence the work reported in this paper.

bell-shaped concentration-dependence, consistent with a role as a signaling scaffold. We further demonstrate using NMR spectroscopy that a polyproline motif within arrestin-3 interacts directly with the SH3 domain of Fgr. To provide a framework for this interaction, we determined the crystal structure of the Fgr SH3 domain at 1.9 Å resolution and developed a model for the GPCR-arrestin-3-Fgr complex that is supported by mutagenesis. This model suggests that Fgr interacts with arrestin-3 at multiple sites and is consistent with the locations of disease-associated Fgr mutations. Collectively, these studies provide a structural framework for arrestin-dependent activation of Fgr

Graphical Abstract

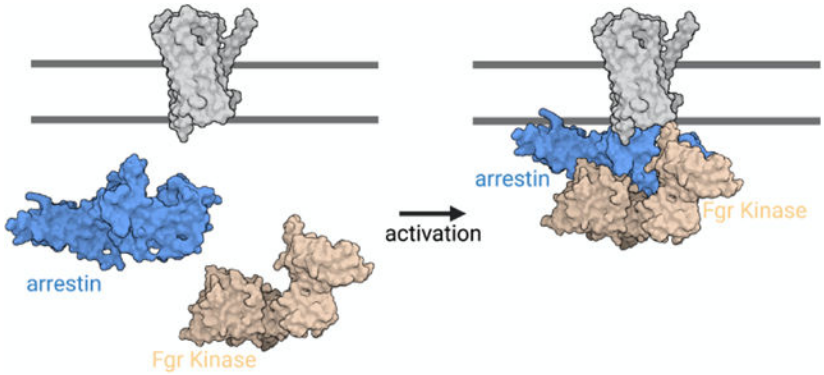

Introduction

The proto-oncogene Fgr belongs to the Src family of tyrosine kinases; its expression is limited to hemopoietic cells (1–3). Fgr regulates the immune response and inflammation (3–7). Physiologically, this contributes to central post-stroke pain (8). Fgr overexpression also promotes the development and rapid progression of acute myeloid leukemia (AML), a type of adult blood cancer (1), as well as ovarian (9) and colorectal (10) cancers. Fgr inhibition or knockdown attenuates cell growth in AML cell lines and in cultured primary cells from AML patients, thus making Fgr an attractive therapeutic target (11,12).

Similar to other Src family kinases, Fgr exhibits a modular organization. The structure of Fgr and all Src family kinases includes a myristoylated N-terminus, a unique region, a Srchomology (SH)3 domain, a SH2 domain, a kinase domain (sometimes called SH1) and a C-terminus that contains an autoinhibitory phospho-tyrosine. Near full-length crystal structures of Src (13,14) and Hck (15,16), and a structurally similar tyrosine kinase Abl (17), revealed that the relative positions of these domains depends upon the kinase activation state. In the autoinhibited inactive conformation, both the SH2 and SH3 domains interact with other sequence regions that stabilize the kinase domains in an inactive conformation and attenuate activity (15,18,19). Specific interactions occur between the SH3 domain and the linker that connects the SH2 and kinase domains and between the SH2 domain and a phospho-tyrosine in the C-terminus Kinase activation includes the phosphorylation of a tyrosine on the activation loop, which has been extensively evaluated in Src (19). Based on close homology between Src and Fgr, phosphorylation of Fgr Tyr-412 is anticipated

to accompany activation (19). Disruption of the autoinhibitory interactions involving the SH3 and SH2 domains promotes a global conformational rearrangement of these domains (14,19).

Src family kinases are activated by binding of regulatory proteins. Some of their binding partners contain polyproline (PxxP) motifs that interact with the SH3 and disrupt kinase autoinhibition. For example, p130Cas (20), HIV-1 Nef (21,22) and focal adhesion kinase (FAK) (23,24) can bind to the SH3 domain of Src, Hck and Lyn, both *in vitro* and in cells. Certain mutations in the Src SH3 domain can also destabilize the autoinhibited state, and increase the cell transforming ability of this kinase (25–27).

High sequence similarity within the Src family suggests a shared mechanism of regulation and activation. Although Fgr regulation is somewhat more enigmatic than that of other Src family kinases, Fgr activity and neutrophil recruitment can be induced following the stimulation of some G protein-coupled receptors (GPCRs). For example, IL8 stimulation of chemokine receptors activates Fgr (28,29). Fgr also regulates arrestin-independent signaling downstream of the stimulated formyl-methionyl-leucyl-phenylalanine peptide (fMLP) receptor 1 (FPR1), which activates neutrophils in response to pathogens (30). Intriguingly, the Fgr kinase also exhibits unusually high basal activity (31). As a result, expression levels may provide a complementary mechanism for controlling Fgr activity, an observation consistent with the increased Fgr expression observed in AML patients (31). The molecular origins of this high basal activity appear to be related to the sequence of the Fgr activation loop, which may allow Fgr to adopt an active conformation spontaneously (31).

Among other pathways, stimulated GPCRs could activate Fgr via bound arrestins. Two arrestins isoforms, called arrestin-2 and arrestin-3, contribute to the GPCR-dependent and -independent activation of hundreds of effectors (32–36). Of these, the first identified arrestin-dependent effector was Src (37). Later, chemokine receptors were shown to initiate Fgr signaling in an arrestin-2-dependent manner (28,29). However, not all GPCR-stimulated Fgr activation is arrestin-dependent; for example, fMLP appears to activate Fgr in an arrestin-independent manner (30).

While the arrestin-dependent activation of Src family kinases is widely accepted, the mechanism of this remains elusive. Conceivably, arrestin binding could disrupt autoinhibition of Src family kinases by an interaction with one of the regulatory domains. Arrestins contain polyproline motifs that could interact with SH3 domains. Consistent with this, mutating the polyproline sequence of arrestin-2 (P91G, P121E) led to decreased Src binding (37).

Here, we propose a model for arrestin-3-dependent Fgr activation. We assessed binding of arrestin-3 to Fgr *in vitro* and determined how arrestin-3 regulates Fgr in cells. We show that arrestin-3 acts as a signaling scaffold in cells and that an arrestin-3-derived polyproline motif binds to the SH3 domain of Fgr. We then combined NMR titration analysis, crystallography, and computational modeling to suggest an architecture of the GPCR-arrestin-3-Fgr complex. This model is supported by the locations of disease-associated mutations in Fgr.

Results

Arrestin-3 scaffolds Fgr

We first explored how arrestin-3 regulates Fgr activity in cells by monitoring arrestin-3-dependent phosphorylation of Fgr Tyr-412. Because a receptor that activates Fgr in an arrestin-dependent manner is not known, we used two forms of arrestin-3 in these experiments as a way to assess arrestin-dependence without a specific receptor stimulated. Full-length arrestin-3 prefers the basal conformation, although it does spontaneously adopt the active conformation at a low level. Truncated arrestin-$3^{(1–393)}$ appears to be pre-activated, i.e. it more readily adopts the active conformation.

We co-expressed either full-length arrestin-3 or arrestin-$3^{(1–393)}$ (38) with Fgr in HEK293 arrestin-2/3 knockout cells. Fgr exhibited high basal activity, as reported (31). However, levels of Fgr Tyr-412 phosphorylation depended on the concentration of both forms of arrestin-3. In the case of full-length arrestin-3, Fgr Tyr-412 phosphorylation increased at intermediate concentrations and decreased at higher concentrations (Fig. 1). The bell-shaped activation curve is a hallmark of a signaling scaffold (39–42) (Fig. 2). This suggests that arrestin-3 contributes to Fgr activation by bridging it with an upstream activator, possibly a GPCR (Fig. 2). In case of arrestin-$3^{(1–393)}$, the curve was shifted to the left relative to that of full-length arrestin-3 (Fig. 1). Increased pFgr was observed at lower concentrations of arrestin-$3^{(1–393)}$, while at the highest concentrations pFgr levels were below that in the absence of transfected arrestin.

The Fgr SH3 domain interacts with a polyproline motif of arrestin-3

To gain mechanistic insight into how arrestin-3 might regulate Fgr activity and to identify the arrestin-3-Fgr interface, we focused on the Fgr SH3 domain. Because SH3 domains interact with proteins containing PxxP polyproline motifs (23,24), we hypothesized that it interacts with a region of arrestin-3 called arrestin Switch I (aSwI, residues 89–99 (43)) (Fig. S1). Notably, the **PP**T**P**N**PP**R**PP** sequence of aSwI contains a double PxxP polyproline motif in the N-to-C-direction and a single polyproline motif in the reverse direction. As aSwI undergoes a conformational change upon arrestin-3 activation, it was suggested to serve as a binding site for some effectors (43).

We combined NMR spectroscopy and X-ray crystallography to probe whether the SH3 domain of Fgr binds to aSwI of arrestin-3. For this, we assigned ^{1}H-^{15}N HSQC resonances of ^{15}N-labeled Fgr SH3 domain using TOCSY-HSQC and NOESY-HSQC spectra of the Fgr SH3 domain (Fig. S2). We titrated the ^{15}N-labeled SH3 domain with peptides corresponding to the **PP**T**P**N**PP**R**PP** sequence of aSwI in arrestin-3 (Fig. 3), using a buffer/DMSO as a negative control. Increasing concentrations of the aSwI peptide of arrestin-3 resulted in chemical shift perturbations in the ^{1}H-^{15}N HSQC spectra consistent with a specific interaction. As no line broadening was observed, we used these chemical shift perturbations to determine the K_D value (Fig. 3), which was found to be 347 ± 106 μM. Because this K_D is too weak to be biologically relevant, the binding of the polyproline motif of arrestin-3 to the SH3 domain of Fgr is likely only part of the full interaction between these two proteins, with additional contacts likely contributing to the binding in the full-length proteins in cells.

The completion of NMR assignments for the SH3 domain allowed us to identify those residues for which resonances shift in response to the arrestin polyproline motif, suggesting those residues are part of the binding site. To identify the elements of the SH3 domain involved in aSwI binding, we next sought to map the NMR-responsive sites into the three-dimensional structure of the SH3 domain, which we determined to 1.9 Å resolution using molecular replacement methods (Fig. 4, Table 1). The structure contains all features expected for an SH3 domain, including five anti-parallel β-strands (β1– β5), three flexible loops (the RT loop, the n-Src loop and the distal loop), and a short 3_{10} helix located near the C-terminus.

Mapping the regions of the isolated Fgr SH3 domain that undergo chemical shift perturbations in the presence of the aSwI peptide (Fig. 4) revealed that these correspond to the Src loop and RT loop, which is the polyproline binding cleft in all SH3 domains characterized to date. This suggests that arrestin-3 interacts with the Fgr SH3 domain using a canonical mode. To validate the polyproline motif in aSwI as a biologically relevant interaction site, we used in-cell assay in arrestin-2/3 knockout HEK293 cells. We co-transfected Fgr and either arrestin-$3^{(1–393)}$ or an arrestin-$3^{(1–393)}$ mutant with the **PP**T**P**N**PP**R**PP**T sequence converted to **AA**T**A**N**AA**R**AA**T via mutagenesis. We found that in contrast to arrestin-$3^{(1–393)}$, the arrestin-$3^{(1–393)}$ mutant lacking the polyproline motif did not affect Fgr Tyr412 phosphorylation in cells (Fig. 5).

We then wanted to perform the converse validation, in this case to identify whether the SH3 domain of Fgr could be involved in regulation of the kinase. For this we used the High-performance Integrated Virtual Environment (HIVE) database (44), a repository for human disease-associated mutations. This identified 155 cancer-associated mutations within the Fgr protein. We mapped those mutations onto the Fgr sequence and found that 24 mutations associated with increased Fgr activity are located in the SH3 domain (residues 77–138) (Fig. 6, Table 2), 30 mutations are located in the SH2 domain (residues 144–241), and 79 mutations are located in the kinase domain (residues 263–516). Interestingly, even though the SH3 domain is the smallest domain, it has the highest rate of cancer-associated mutations. This supports the idea that mutations in the SH3 domain decrease the stability of the autoinhibited conformation of Fgr.

A model for the interaction between Fgr and arrestin-3

To understand how arrestin promotes Fgr activation, we integrated our data and inferences with known poses of Src family kinases to develop a data-guided computational model of the interaction between Fgr and arrestin-3. To propose how an isolated arrestin-3 polyproline sequence could interact with the SH3 domain, we compared the Fgr SH3 domain structure with SH3 domain structures from Src (PDB: 1QWE, 1QWF (13)) and Abl (PDB:1BBZ (45)) bound to polyproline-containing peptides. Here, we considered that the arrestin-3 polyproline motif is one of the regions of arrestin that undergoes substantial conformational change upon transition from the basal to the active conformation; in fact, this conformational change results in a maximal displacement of 5.8 Å (43). In the intact system with full-length arrestin, we speculate that the sequence corresponding to our peptide adopts an active-like conformation. Because isolated peptides are free to adopt a broader range of conformations

than the same sequences within a protein, we hypothesize that interaction between the SH3 domain and the isolated peptide induces a conformation similar to that observed in the context of active arresitn-3. Docking was therefore performed using the peptide in the conformation observed in the active arrestin-3 structure (43)and with arrestin-3 in the active conformation, iterating along the polyproline sequence in both the N- to C- and C- to N-orientations. This suggested several plausible modes of interaction for the isolated peptide that satisfy the NMR titration data (Fig. S3).

We next evaluated possible binding modes of the aSwI sequence to the Fgr SH3 domain within the context of folded arrestin-3 (43). We eliminated models that had substantial steric overlap between the arrestin-3 and the isolated SH3 domain, which excluded all models where the interaction involved the first polyproline motif of aSwI. This suggested that the second polyproline motif found in the arrestin-3 aSwI was more likely to interact with SH3 domain than the first polyproline motif in this arrestin structural element.

We next developed a homology model of near full-length Fgr in both the inactive and active conformations using the equivalent poses from crystal structures of Src kinase (PDB: 1Y57 (Fig. S4) (13,14)). We used all possible isolated SH3-arrestin-3 interactions to identify which would be consistent with different potential conformations of Fgr kinase. This identified four docked poses consistent with the active conformation. As no structures of receptor-bound arrestin-3 are available, each of these models was then overlaid with the cryoEM structure of arrestin-2 bound to the M2 muscarinic receptor (46). Models in which Fgr kinase sterically overlapped with the membrane were excluded. Remaining models were energy minimized (Fig. 7).

At a conceptual level, the models are roughly equivalent and involve intimate contacts between both domains of arrestin-3 and all three domains of the kinase: the kinase domain, SH2, and SH3. Perhaps the most interesting aspect of these models is the extensive interaction found between arrestin-3 and the kinase domain, consistent with previous findings that identified the kinase domain as a point of contact in the arrestin-2-Src interaction (47). In addition, all models contained a positively charged patch of residues on Fgr that approached the predicted location of the membrane, suggesting a possible peripheral site of membrane interaction in the intact complex. These residues were bound to sulfates in the crystal structure of Src kinase (13,14).

Discussion

It has been over two decades since arrestins were shown to serve as signal tranducers (37). Src kinase was the first identified arrestin-dependent effector (37), and hundreds of additional effectors have been subsequently reported (48,49). These effectors tend to be master regulators of cell growth, proliferation, and migration, and include Src family kinases (50–52), mitogen activated protein kinases (53,54), leucine zipper kinases (55–57), and many others. Despite the clear importance of arrestins in initiating signaling, a structural depiction of the underlying signaling complexes remains elusive.

Here, we used a hybrid approach to understand how arrestin-3 contributes to Fgr activation, a kinase the contributes to cellular fine-tuning of biological processes via post-translational modifications, in this case, via protein phosphorylation (58). Cellular assays show a modest yet statistically significant arrestin-3-dependence of Fgr phosphorylation (Fig. 1). Conceivably, the changes of Fgr phosphorylation might be modest because we did not activate an upstream receptor; the identity of an upstream receptor(s) that promote arrestin-3-Fgr interaction is not known. However, the replacement of full-length arrestin-3 with pre-activated arrestin-$3^{(1–393)}$ mutant yielded a left shift of the dose-response curve but no increase in the maximum level of phosphorylated Fgr (Fig. 1). This would instead suggest that a similar activation level would be observed even in the presence of an appropriately stimulated receptor, but that the kinetics of activation would differ. It is important to keep in mind that levels of kinase activation do not need to be large in magnitude to be biologically relevant. A single phosphorylation event on a kinase such as this may allow substantial downstream changes because it greatly increases cellular kinase activity (59). In fact, small changes in protein phosphorylation patterns are associated with development of diseases like cancer and neurogenerative disease (60).

Regardless of the absolute levels of phosphorylated Fgr, the bell-shaped dependence of Fgr activation on arrestin-3 concentration and the left-shift associated with pre-active arrestin (Fig. 1) suggests that arrestin acts as a scaffold that bridges Fgr with an upstream activator (Fig. 2). This mode of binding is consistent with prior observations that arrestins can act as a bridge between other Src family kinases and activated GPCRs (37,61–63,47). We showed that arrestin-3 binds directly to the Fgr SH3 domain (Fig. 3). This suggests that the SH3 domain of Fgr contributes to arrestin-dependent activation. This is consistent with studies that show excess SH3 can block Src kinase activation and the interaction between Src and arrestin (37,47). It is also consistent with the identification of Fgr SH3 domain mutations associated with cancer (Table 2), where a subset map to the proposed arrestin-3-Fgr interface (Fig. 4). The moderate affinity that we observe between the isolated Fgr SH3 domain and a peptide containing the arrestin-3 aSwI sequence suggests that this interaction is only one of several contacts between arrestin-3 and Fgr. In fact, past studies showed that mutations of the polyproline motif in arrestin-2 (P91G, P121E) decreased, but did not abolish, the interaction with Src (37,64), suggesting that at least one additional peripheral interaction site contributes to binding.

We synthesized all these observations into a model for a GPCR-arrestin-3-Fgr signal initiation complex. Our model (Fig. 7), suggests intimate interactions between all domains of Fgr and arrestin-3. This is consistent with a recent report that the kinase domain of Src kinase binds arrestin-2 (47). This is potentially inconsistent, however, with previous studies demonstrating that neither the isolated Src kinase domain nor the SH2 domain inhibit the interaction between arrestin-2 and Src (37,47), which could be interpreted as lack of the role of these domains in complex formation. The potential interface between arrestin-3 polyproline region and the Fgr SH3 domain is supported by the location of numerous cancer-associated mutations (Table 2). The residues A90, R91, T92, E93, D94, and E11 located in this arrestin-Fgr interface in our model are mutated in cancer.

The question arises as to whether the presented arrestin-3-Fgr model might serve as a basis for a complex between other Src family kinases and an arrestins. Although possible, arrestins exhibit broad selectivity for their binding partners and the limited data available suggests that the two non-visual arrestins might bind to both their activators and their effectors differently. For example, in structures of the arrestin-2-β2-adrenergic receptor and the arrestin-2-neurotensin receptor 1 complexes arrestin-2 was found in quite different orientations relative to bound GPCR (65,66). Moreover, all available data suggest that the two isoforms of non-visual arrestin, which are 78% identical, interact with the mitogen activated protein kinase ERK2 differentially (67). High-resolution experimental structures of signal initiation complexes between GPCRs, arrestins, and different Src family kinases will be necessary to test this.

Nevertheless, our data and model reveal a possible mechanism of arrestin binding that can activate Fgr and suggest basic mechanisms of Fgr-dependent signal initiation. Considering the documented role of excessive activity of Fgr in AML, this model might provide a framework for developing new therapeutics.

Materials and Methods

Cloning, Expression, and Purification of the Fgr SH3 domain.

The cDNA encoding the human Fgr SH3 domain was inserted into pET24 vector which added a C-terminal His_6 affinity tag. This plasmid was transformed into *Escherichia coli* BL21(*DE3*). Transformed cells were grown in Luria-Bertani (LB) broth at 37 °C until the OD_{600} reached 0.4–0.8. Protein expression was induced with 1 mM IPTG at 30 °C for 4 hr. The cells were harvested by centrifugation at 9,180 × *g* (15 min, 4 °C) and the pellets were stored at −80 °C. The cells were resuspended in lysis buffer (50 mM Tris pH 7.5, 1 mM EDTA, 150 mM NaCl, 2 mM $MgCl_2$, 1 mM TCEP, plus lysozyme) containing bacterial protease inhibitor cocktail (Sigma) and Deoxyribonuclease I from bovine pancreas (DNAse I, Sigma, St. Louis, MO). The resuspended cells were lysed by sonication (5 sec on/off pulse, 10 minutes, 75% intensity) (sonicator model FB505; Thermo Fisher Scientific, Waltham, MA), after which the cell debris was pelleted (38,360 × *g*, 1 hr, 4 °C). The clarified lysate was loaded on a HisTrap HP column (Catalog # 17-5255-01, Cytivia, Marlborough, MA). The column was washed with at least 10 column volumes of equilibration buffer (50 mM Tris pH 7.5, 150 mM NaCl, 10% glycerol, 25 mM imidazole) and the protein was eluted with a gradient of 25–250 mM imidazole. The eluted protein was further purified and exchanged into storage buffer (20 mM MES pH 7.5, 100 mM NaCl, 1 mM TCEP) using a Superdex 200 increase 10/300 GL column (Catalog#GE28-9909-44, Cytivia, Marlborough, MA). Purified protein was aliquoted, flash frozen in liquid nitrogen and stored at −80 °C.

Arrestin purification.

Full-length arrestin-3 and its truncated (1–393) mutant were expressed in *E. coli* and purified as previously described (68).

Crystallization.

The purified Fgr SH3 domain was concentrated to 4.5 mg/ml in 20 mM MES pH 7.5, 100 mM NaCl, 1 mM TCEP. Crystals were grown using the sitting drop vapor diffusion method at 23 °C by mixing the protein (4.5 mg/mL) in a 1:1 ratio with the reservoir solution (100 mM NaCitrate tribasic, 100 mM citric acid, pH 5.5, and 40% (v/v) PEG 600). Crystals were flash cooled without additional cryo protectant by plunging in liquid nitrogen.

Data collection, structure determination, refinement and analysis.

Diffraction data were collected at 100 K at the Stanford Synchrotron Radiation Lightsource (SSRL) beamline BL9–2 using a wavelength of 0.97946 Å and a DECTRIS PILATUS 6M detector. Data were processed and scaled using HKL2000 (69). The structure was determined by molecular replacement in the PHASER (70) subroutine of PHENIX (71), using the SH3 domain of the Src-related non-receptor tyrosine kinase, Yes as the search model (**PDB: 2HDA** (72)). The structure was refined using PHENIX (71) and improved by model building in COOT(73). Data collection and refinement statistics are summarized in Table 1.

NMR spectroscopy.

The Fgr SH3 domain was uniformly ^{15}N-labelled using standard techniques. Briefly, the preculture was grown in LB media and 1 ml of this culture was used to inoculate 1 L minimal media with the following composition 6 g/L Na_2HPO_4, 3 g/L KH_2PO_4, 0.5 g/L NaCl, 1 g/L ^{15}N NH_4Cl, 0.1 M $CaCl_2$, 1M $MgSO_4$, 40% glucose and 10 ml vitamin solution (Cellgro). Cells were grown overnight at room temperature (approximately 20 °C). Then protein expression was induced using 1 mM IPTG at cell density OD_{600} of 0.7–0.8. After 18 – 20 h of protein expression at room temperature, cells were harvested by centrifugation at 7000 *g* for 10 min at 4 °C and the pellets were frozen at −80 °C. Cell lysis and protein purification were performed as described for unlabeled SH3 domains.

NMR experiments were performed using a Bruker DRX 600 MHz spectrometer and a sample buffer containing 20 mM MOPS, 150 mM NaCl, 1 mM TCEP, pH 7.5 and at 298K. ^{1}H-^{15}N HSQC spectra were recorded using the standard Bruker hsqcetfpf3gpsi2 pulse sequence. These assignments were verified by TOCSY-HSQC (dipsihsqcf3gpwg3d) and NOESY-HSQC (noesyhsqcetf3gp3d) spectra recorded using standard pulse sequences. For the Fgr SH3 domains, complete assignments were made using TOCSY-HSQC and NOESY-HSQC pulse sequences and an ^{15}N-SH3 domain concentration of 500 μM.

For titration of the arrestin-derived peptides, 500 μM ^{15}N-SH3 domain was used, and the peptide concentration was varied from 50 μM to 1500 μM. Data were processed using TOPSPIN and analyzed with SPARKY (74). The observed peptide-induced chemical shift perturbations (Δδ) were measured and analyzed using equation 1 and the shifting residues were quantified by equation 2, where X is total ligand, Y is total binding in Δδ, B_{Max} is maximum binding in the Δδ units (Δδ at saturation),, K_D is the projected dissociation constant from fitting the curve, and NS*X is a linear term to account for nonspecific shifts due to DMSO effects / nonspecific shifts. Fitting of the data yielded a K_D value for each interacting pair (Figure 3).

$$\Delta\delta_{ppm} = \sqrt{(\Delta\delta_{HN})^2 + \left(\frac{\Delta\delta_N}{6.51}\right)^2} \quad \text{equation 1}$$

$$Y = Bmax * X/(K_D + X) + NS * X \quad \text{equation 2}$$

$$Standard\ Error\ (SE) = \frac{sample\ standard\ deviation}{\sqrt{number\ of\ samples}} \quad \text{equation 3}$$

$$Total\ Standard\ Error\ for\ K_D = \sqrt{SE_1^2 + SE_2^2 + SE_3^2} \quad \text{equation 4}$$

High-performance Integrated Virtual Environment (HIVE) search.

The HIVE search was performed as previously described (44). The Uniprot ID for the human Fgr kinase was used in the search bar to find single-nucleotide variations (SNVs) (Uniprot ID P09769 FGR_HUMAN). https://hive.biochemistry.gwu.edu/biomuta/norecord

Docking and molecular dynamics.

The crystal structure of C-Src SH3 domain (PDB 1QWF) was used as a template to position the polyproline peptide in the SH3 domain of the Fgr kinase using MOE (75). This structure was simulated with molecular dynamics (MD) using the Amber14 ff14SB force-field parameters (76,77). The protein was solvated in TIP3P (78) octahedral box with a 10 Å buffer of water around the protein in each direction and Na^+ and Cl^- counterions were added to neutralize surface protein charges. In the first step, the protein structure was held fixed with a force constant of 500 kcal mol^{-1} $Å^{-2}$ while the system was minimized with 500 steps of steepest descent followed by 500 steps with the conjugate gradient method. In the second step, the restraints on the protein were removed and 1000 steps of steepest descent minimization were performed followed by 1500 steps of conjugate gradient. The system was then heated to 300 K with MD while holding the protein fixed with a force constant of 10 kcal mol^{-1} $Å^{-2}$ for 1000 steps. Then, the restraints were removed, and 1000 MD steps were performed. The SHAKE algorithm (79) was used to constrain all bonds involving hydrogen in the simulations. 25 ns production MD was performed at 300 K using the NPT ensemble and a 2 fs time step with nonbonded cutoff of 10 Å. The temperature was fixed with the Langevin dynamics thermostat (80) and the pressure was fixed with a Monte Carlo barostat (81). The snapshots generated from MD were clustered using hierarchical clustering method in Pytraj package (82).

Model of the GPCR-arrestin-kinase interaction.

ClusPro2.0 (83–85) was used to dock Src kinase (PDB: 1y57)(14) and arrestin-3 (PDB: 5tv1) (43). Missing hydrogens, sidechains, and loops of both the structures were prepared using MOE (86). Src kinase and arrestin-3 were considered as receptor and ligand, respectively. In ClusPro, the ligand was rotated 70,000 times and for each rotation, the ligand was translated in the X, Y, Z axes relative to the receptor on a grid. ClusPro

parameters for ‘Receptor Attraction’ were chosen as a-91 and for ‘Ligand Attraction’ were chosen as a-89 a-90 a-91 a-92 a-93 a-94 a-95 a-96 a-97 a-98 to guide the docking. The top “balanced” model was simulated and clustered following the protocol described above. The structures were then superposed onto the cryoEM structure of arrestin-2 with the muscarinic M2 receptor (PDB: 6U1N, (46))

Synthesis of pcDNA3.1 encoding wild-type and mutant full-length Fgr.

For the phosphorylation assay, the full length wild-type and mutant Fgr constructs were produced by GenScript and confirmed by dideoxy sequencing. The ORF clone (OHu28536D) was purchased in a pcDNA3.1^{+}/C-(K)-DYK mammalian expression cloning vector.

FGR phosphorylation in HEK293 arrestin-2/3 knockout cells.

HEK293 arrestin-2/3 knockout cells (38) were maintained in Dulbecco’s modified Eagle’s media (DMEM) (Thermo Fisher Scientific, Waltham, MA) containing 10% fetal bovine serum (FBS) (Thermo Fisher Scientific, Waltham, MA), penicillin (100 IU/mL) and streptomycin (100 mg/mL) at 37°C and 5% CO_2. Cells were transfected at 90–100% confluency in 6-well plates with Lipofectamine 2000 (Thermo Fisher Scientific, Waltham, MA) using a 2:1 ratio of Lipofectamine:DNA. The media was change to Opti-MEM prior to transfection and the cells were co-transfected with either full-length arrestin-3 or arrestin-3$^{1–393}$ in pcDNA3.1 and full-length Fgr (0.05 μg). Empty pCDNA3.1 vector was added to bring the total to 1.8 μg DNA transfected per well. The cells were then lysed with 300 μL of 2x SDS sample buffer. Lysates were loaded on a 10% SDS-PAGE gel, separated by electrophoresis, followed by a dry membrane transfer (15 V, 7 min) using an iBlot 2 Gel transfer device (Thermo Fisher Scientific, Waltham, MA). The membranes were blocked with 5% non-fat dry milk in 1x TBST for 1 hour, washed with 1x TBST (3x, 5 min each) and incubated with the respective primary antibodies overnight at 4 °C. Rabbit polyclonal antibodies against arrestin (F431 antibody; (38)), total Fgr (Thermo Fisher Scientific, Waltham, MA), and phospho-Fgr (Tyr412, Thermo Fisher Scientific, Waltham, MA). The following day, the membranes were washed with 1x TBST (3x, 5 min) and incubated with HRP-conjugated anti-rabbit secondary antibody (1:10,000, Seracare Life Sciences Inc, Milford, MA) for 1 h at room temperature. The secondary antibody was washed with 1x TBST (3x, 5 min). Protein bands were visualized using the SuperSignal West Pico PLUS Chemiluminescent Substrate (Thermo Fisher Scientific, Waltham, MA) followed by imaging using the Bio-Rad Gel Doc Imager with enhanced chemiluminescence (Catalog # 32109, Thermo Fisher Scientific, Waltham, MA). Bands were quantified using the Image Studio Lite software (LI-COR Biosciences).

Supplementary Material

Refer to Web version on PubMed Central for supplementary material.

Acknowledgments

Supported in part by National Institutes of Health (NIH) grants (GM120569 (TMI), DA043680 (TMI), R35 GM122491 (VVG), R01 EY011500 (VVG), the Louise B McGavock Chair (TMI) and Vanderbilt University

Cornelius Vanderbilt Chair (VVG), RF1 AG056147 (CRS) Molecular Biophysics Training Grant from the NIH 2T32GM008320-31 (IP), and F31 AG0694662-01 (MAC). This material is based upon work supported by the National Science Foundation Graduate Research Fellowship Program under Grant No. 1937963 (IP) and DGE-1445197 (MAC). Any opinions, findings, and conclusions or recommendations expressed in this material are those of the author(s) and do not necessarily reflect the views of the NIH or the National Science Foundation. This work used Vanderbilt's NMR facility supported in part by grants for NMR instrumentation from the NSF (0922862), NIH (S10 RR025677) and Vanderbilt University matching funds. We thank Dr. Markus W. Voehler for assistance in NMR data collection and NMR facility maintenance.

Bibliography

1. Willman CL, Stewart CC, Griffith JK, Stewart SJ, Tomasi TB. Differential expression and regulation of the c-src and c-fgr protooncogenes in myelomonocytic cells. PNAS. 1987 Jul 1;84(13):4480–4. [PubMed: 2440024]
2. Brickell PM, Patel M. Structure and expression of c-fgr protooncogene mRNA in Epstein-Barr virus converted cell lines. Br J Cancer. 1988 Dec;58(6):704–9. [PubMed: 2852026]
3. Inoue K, Yamamoto T, Toyoshima K. Specific expression of human c-fgr in natural immunity effector cells. Mol Cell Biol. 1990 Apr;10(4):1789–92. [PubMed: 2181286]
4. Abe K, Cox A, Takamatsu N, Velez G, Laxer RM, Tse SML, et al. Gain-of-function mutations in a member of the Src family kinases cause autoinflammatory bone disease in mice and humans. PNAS. 2019 Jun 11;116(24):11872–7. [PubMed: 31138708]
5. Lowell CA, Soriano P, Varmus HE. Functional overlap in the src gene family: inactivation of hck and fgr impairs natural immunity. Genes Dev. 1994 Feb 15;8(4):387–98. [PubMed: 8125254]
6. Rohwedder I, Kurz ARM, Pruenster M, Immler R, Pick R, Eggersmann T, et al. Src family kinase-mediated vesicle trafficking is critical for neutrophil basement membrane penetration. Haematologica. 2020 Jul;105(7):1845–56. [PubMed: 31699792]
7. Acín-Pérez R, Iborra S, Martí-Mateos Y, Cook ECL, Conde-Garrosa R, Petcherski A, et al. Fgr kinase is required for proinflammatory macrophage activation during diet-induced obesity. Nature Metabolism. 2020 Sep;2(9):974–88.
8. Huang T, Fu G, Gao J, Zhang Y, Cai W, Wu S, et al. Fgr contributes to hemorrhage-induced thalamic pain by activating NF-κB/ERK1/2 pathways. JCI Insight [Internet]. 2020 Oct 15 [cited 2020 Dec 24];5(20). Available from: https://insight.jci.org/articles/view/139987
9. Kim H-S, Han HD, Armaiz-Pena GN, Stone RL, Nam EJ, Lee J-W, et al. Functional Roles of Src and Fgr in Ovarian Carcinoma. Clinical Cancer Research. 2011 Apr 1;17(7):1713–21. [PubMed: 21300758]
10. Roseweir AK, Powell AGMT, Horstman SL, Inthagard J, Park JH, McMillan DC, et al. Src family kinases, HCK and FGR, associate with local inflammation and tumour progression in colorectal cancer. Cellular Signalling. 2019 Apr 1;56:15–22. [PubMed: 30684564]
11. Dos Santos C, McDonald T, Ho YW, Liu H, Lin A, Forman SJ, et al. The Src and c-Kit kinase inhibitor dasatinib enhances p53-mediated targeting of human acute myeloid leukemia stem cells by chemotherapeutic agents. Blood. 2013 Sep 12;122(11):1900–13. [PubMed: 23896410]
12. Weir MC, Shu ST, Patel RK, Hellwig S, Chen L, Tan L, et al. Selective Inhibition of the Myeloid Src-Family Kinase Fgr Potently Suppresses AML Cell Growth in Vitro and in Vivo. ACS Chem Biol. 2018 15;13(6):1551–9. [PubMed: 29763550]
13. Feng S, Kasahara C, Rickles RJ, Schreiber SL. Specific interactions outside the proline-rich core of two classes of Src homology 3 ligands. PNAS. 1995 Dec 19;92(26):12408–15. [PubMed: 8618911]
14. Cowan-Jacob SW, Fendrich G, Manley PW, Jahnke W, Fabbro D, Liebetanz J, et al. The Crystal Structure of a c-Src Complex in an Active Conformation Suggests Possible Steps in c-Src Activation. Structure. 2005 Jun 1;13(6):861–71. [PubMed: 15939018]
15. Sicheri F, Moarefi I, Kuriyan J. Crystal structure of the Src family tyrosine kinase Hck. Nature. 1997 Feb;385(6617):602–9. [PubMed: 9024658]
16. Schindler T, Sicheri F, Pico A, Gazit A, Levitzki A, Kuriyan J. Crystal Structure of Hck in Complex with a Src Family–Selective Tyrosine Kinase Inhibitor. Molecular Cell. 1999 May 1;3(5):639–48. [PubMed: 10360180]

17. Schindler T Structural Mechanism for STI-571 Inhibition of Abelson Tyrosine Kinase. Science. 2000 Sep 15;289(5486):1938–42. [PubMed: 10988075]

18. Xu W, Doshi A, Lei M, Eck MJ, Harrison SC. Crystal structures of c-Src reveal features of its autoinhibitory mechanism. Mol Cell. 1999 May;3(5):629–38. [PubMed: 10360179]

19. Xu W, Harrison SC, Eck MJ. Three-dimensional structure of the tyrosine kinase c-Src. Nature. 1997 Feb 13;385(6617):595–602. [PubMed: 9024657]

20. Nakamoto T, Sakai R, Ozawa K, Yazaki Y, Hirai H. Direct Binding of C-terminal Region of p130 to SH2 and SH3 Domains of Src Kinase. J Biol Chem. 1996 Apr 12;271(15):8959–65. [PubMed: 8621540]

21. Briggs SD, Sharkey M, Stevenson M, Smithgall TE. SH3-mediated Hck tyrosine kinase activation and fibroblast transformation by the Nef protein of HIV-1. J Biol Chem. 1997 Jul 18;272(29):17899–902. [PubMed: 9218412]

22. Trible RP, Emert-Sedlak L, Smithgall TE. HIV-1 Nef Selectively Activates Src Family Kinases Hck, Lyn, and c-Src through Direct SH3 Domain Interaction. J Biol Chem. 2006 Sep 15;281(37):27029–38. [PubMed: 16849330]

23. Moroco JA, Baumgartner MP, Rust HL, Choi HG, Hur W, Gray NS, et al. A Discovery Strategy for Selective Inhibitors of c-Src in Complex with the Focal Adhesion Kinase SH3/SH2-binding Region. Chem Biol Drug Des. 2015 Aug;86(2):144–55. [PubMed: 25376742]

24. Thomas JW, Ellis B, Boerner RJ, Knight WB, White GC, Schaller MD. SH2- and SH3-mediated Interactions between Focal Adhesion Kinase and Src. J Biol Chem. 1998 Jan 2;273(1):577–83. [PubMed: 9417118]

25. Erpel T, Superti-Furga G, Courtneidge SA. Mutational analysis of the Src SH3 domain: the same residues of the ligand binding surface are important for intraand intermolecular interactions. EMBO J. 1995 Mar 1;14(5):963–75. [PubMed: 7534229]

26. Wages DS, Keefer J, Rall TB, Weber MJ. Mutations in the SH3 domain of the src oncogene which decrease association of phosphatidylinositol 3'-kinase activity with pp60v-src and alter cellular morphology. J Virol. 1992 Apr;66(4):1866–74. [PubMed: 1312609]

27. Weng Z, Rickles RJ, Feng S, Richard S, Shaw AS, Schreiber SL, et al. Structure-function analysis of SH3 domains: SH3 binding specificity altered by single amino acid substitutions. Mol Cell Biol. 1995 Oct;15(10):5627–34. [PubMed: 7565714]

28. Barlic J, Andrews JD, Kelvin AA, Bosinger SE, DeVries ME, Xu L, et al. Regulation of tyrosine kinase activation and granule release through β-arrestin by CXCR1. Nature Immunology. 2000 Sep;1(3):227–33. [PubMed: 10973280]

29. Mazzi P, Caveggion E, Lapinet-Vera JA, Lowell CA, Berton G. The Src-Family Kinases Hck and Fgr Regulate Early Lipopolysaccharide-Induced Myeloid Cell Recruitment into the Lung and Their Ability To Secrete Chemokines. JI. 2015 Sep 1;195(5):2383–95.

30. Fumagalli L, Zhang H, Baruzzi A, Lowell CA, Berton G. The Src Family Kinases Hck and Fgr Regulate Neutrophil Responses to N-Formyl-Methionyl-Leucyl-Phenylalanine. J Immunol. 2007 Mar 15;178(6):3874–85. [PubMed: 17339487]

31. Shen K, Moroco JA, Patel RK, Shi H, Engen JR, Dorman HR, et al. The Src family kinase Fgr is a transforming oncoprotein that functions independently of SH3-SH2 domain regulation. Sci Signal. 2018 23;11(553).

32. Chen Q, Iverson TM, Gurevich VV. Structural Basis of Arrestin-Dependent Signal Transduction. Trends in Biochemical Sciences. 2018 Jun 1;43(6):412–23. [PubMed: 29636212]

33. Tian X, Kang DS, Benovic JL. β-arrestins and G Protein-Coupled Receptor Trafficking. Handb Exp Pharmacol. 2014;219:173–86. [PubMed: 24292830]

34. DeWire SM, Ahn S, Lefkowitz RJ, Shenoy SK. β-Arrestins and Cell Signaling. Annual Review of Physiology. 2007;69(1):483–510.

35. Peterson YK, Luttrell LM. The Diverse Roles of Arrestin Scaffolds in G Protein-Coupled Receptor Signaling. Pharmacol Rev. 2017;69(3):256–97. [PubMed: 28626043]

36. Gurevich VV, Gurevich EV. GPCR Signaling Regulation: The Role of GRKs and Arrestins. Front Pharmacol [Internet]. 2019 [cited 2021 Jan 8];10. Available from: https://www.frontiersin.org/articles/10.3389/fphar.2019.00125/full

37. Luttrell LM, Ferguson SSG, Daaka Y, Miller WE, Maudsley S, Rocca GJD, et al. β-Arrestin-Dependent Formation of β2 Adrenergic Receptor-Src Protein Kinase Complexes. Science. 1999 Jan 29;283(5402):655–61. [PubMed: 9924018]
38. Alvarez-Curto E, Inoue A, Jenkins L, Raihan SZ, Prihandoko R, Tobin AB, et al. Targeted Elimination of G Proteins and Arrestins Defines Their Specific Contributions to Both Intensity and Duration of G Protein-coupled Receptor Signaling. J Biol Chem. 2016 Dec 30;291(53):27147–59. [PubMed: 27852822]
39. Kook S, Zhan X, Kaoud TS, Dalby KN, Gurevich VV, Gurevich EV. Arrestin-3 Binds c-Jun N-terminal Kinase 1 (JNK1) and JNK2 and Facilitates the Activation of These Ubiquitous JNK Isoforms in Cells via Scaffolding. J Biol Chem. 2013 Dec 27;288(52):37332–42. [PubMed: 24257757]
40. Song X, Coffa S, Fu H, Gurevich VV. How Does Arrestin Assemble MAPKs into a Signaling Complex? J Biol Chem. 2009 Jan 2;284(1):685–95. [PubMed: 19001375]
41. Zhan X, Perez A, Gimenez LE, Vishnivetskiy SA, Gurevich VV. Arrestin-3 binds the MAP kinase JNK3α2 via multiple sites on both domains. Cellular Signalling. 2014 Apr 1;26(4):766–76. [PubMed: 24412749]
42. Zhan X, Kaoud TS, Kook S, Dalby KN, Gurevich VV. JNK3 Enzyme Binding to Arrestin-3 Differentially Affects the Recruitment of Upstream Mitogen-activated Protein (MAP) Kinase Kinases. J Biol Chem. 2013 Oct 4;288(40):28535–47. [PubMed: 23960075]
43. Chen Q, Perry NA, Vishnivetskiy SA, Berndt S, Gilbert NC, Zhuo Y, et al. Structural basis of arrestin-3 activation and signaling. Nature Communications. 2017 Nov 10;8(1):1427.
44. Wu T-J, Shamsaddini A, Pan Y, Smith K, Crichton DJ, Simonyan V, et al. A framework for organizing cancer-related variations from existing databases, publications and NGS data using a High-performance Integrated Virtual Environment (HIVE). Database (Oxford). 2014;2014:bau022. [PubMed: 24667251]
45. Pisabarro MT, Serrano L, Wilmanns M. Crystal structure of the abl-SH3 domain complexed with a designed high-affinity peptide ligand: implications for SH3-ligand interactions11Edited by I Wilson. Journal of Molecular Biology. 1998 Aug 21;281(3):513–21. [PubMed: 9698566]
46. Staus DP, Hu H, Robertson MJ, Kleinhenz ALW, Wingler LM, Capel WD, et al. Structure of the M2 muscarinic receptor-β-arrestin complex in a lipid nanodisc. Nature. 2020 Mar;579(7798):297–302. [PubMed: 31945772]
47. Pakharukova N, Masoudi A, Pani B, Staus DP, Lefkowitz RJ. Allosteric activation of proto-oncogene kinase Src by GPCR-beta-arrestin complexes. J Biol Chem. 2020 Sep 25;
48. Shenoy SK, McDonald PH, Kohout TA, Lefkowitz RJ. Regulation of Receptor Fate by Ubiquitination of Activated 2-Adrenergic Receptor and -Arrestin. 2001;294:8.
49. Xiao K, McClatchy DB, Shukla AK, Zhao Y, Chen M, Shenoy SK, et al. Functional specialization of beta-arrestin interactions revealed by proteomic analysis. Proc Natl Acad Sci USA. 2007 Jul 17;104(29):12011–6. [PubMed: 17620599]
50. Felsenfeld DP, Schwartzberg PL, Venegas A, Tse R, Sheetz MP. Selective regulation of integrin–cytoskeleton interactions by the tyrosine kinase Src. Nat Cell Biol. 1999 Aug;1(4):200–6. [PubMed: 10559917]
51. Johnson D, Agochiya M, Samejima K, Earnshaw W, Frame M, Wyke J. Regulation of both apoptosis and cell survival by the v-Src oncoprotein. Cell Death Differ. 2000 Aug;7(8):685–96. [PubMed: 10918442]
52. Riley D, Carragher NO, Frame MC, Wyke JA. The mechanism of cell cycle regulation by v-Src. Oncogene. 2001 Sep;20(42):5941–50. [PubMed: 11593401]
53. Srinivasa S, Doshi P. Extracellular signal-regulated kinase and p38 mitogen-activated protein kinase pathways cooperate in mediating cytokine-induced proliferation of a leukemic cell line. Leukemia. 2002 Feb;16(2):244–53. [PubMed: 11840291]
54. Boutros T, Chevet E, Metrakos P. Mitogen-Activated Protein (MAP) Kinase/MAP Kinase Phosphatase Regulation: Roles in Cell Growth, Death, and Cancer. Pharmacol Rev. 2008 Sep;60(3):261–310. [PubMed: 18922965]

55. Ganguly R, Mohyeldin A, Thiel J, Kornblum HI, Beullens M, Nakano I. MELK—a conserved kinase: functions, signaling, cancer, and controversy. Clin Transl Med. 2015 Mar 7;4:11. [PubMed: 25852826]
56. Chen M, Geoffroy CG, Wong HN, Tress O, Nguyen MT, Holzman LB, et al. Leucine Zipper-bearing Kinase promotes axon growth in mammalian central nervous system neurons. Sci Rep. 2016 Aug;6(1):31482. [PubMed: 27511108]
57. Perry NA, Fialkowski KP, Kaoud TS, Kaya AI, Chen AL, Taliaferro JM, et al. Arrestin-3 interaction with maternal embryonic leucine-zipper kinase. Cellular Signalling. 2019 Nov 1;63:109366. [PubMed: 31352007]
58. Karve TM, Cheema AK. Small Changes Huge Impact: The Role of Protein Posttranslational Modifications in Cellular Homeostasis and Disease. Journal of Amino Acids. 2011 Jul 21;2011:e207691.
59. Nishi H, Shaytan A, Panchenko AR. Physicochemical mechanisms of protein regulation by phosphorylation. Frontiers in Genetics. 2014;5:270. [PubMed: 25147561]
60. Seo J, Park M. Molecular crosstalk between cancer and neurodegenerative diseases. Cell Mol Life Sci. 2020 Jul;77(14):2659–80. [PubMed: 31884567]
61. Cao W, Luttrell LM, Medvedev AV, Pierce KL, Daniel KW, Dixon TM, et al. Direct Binding of Activated c-Src to the β3-Adrenergic Receptor Is Required for MAP Kinase Activation *. Journal of Biological Chemistry. 2000 Dec 8;275(49):38131–4.
62. Yang M, Zhang H, Voyno-Yasenetskaya T, Ye RD. Requirement of Gβγ and c-Src in D2 Dopamine Receptor-Mediated Nuclear Factor-κB Activation. Mol Pharmacol. 2003 Aug 1;64(2):447–55. [PubMed: 12869650]
63. Kaya AI, Perry NA, Gurevich VV, Iverson TM. Phosphorylation barcode-dependent signal bias of the dopamine D1 receptor. PNAS. 2020 Jun 23;117(25):14139–49. [PubMed: 32503917]
64. Miller WE, Maudsley S, Ahn S, Khan KD, Luttrell LM, Lefkowitz RJ. β-Arrestin1 Interacts with the Catalytic Domain of the Tyrosine Kinase c-SRC ROLE OF β-ARRESTIN1-DEPENDENT TARGETING OF c-SRC IN RECEPTOR ENDOCYTOSIS. J Biol Chem. 2000 Apr 14;275(15):11312–9. [PubMed: 10753943]
65. Nguyen AH, Thomsen ARB, Cahill TJ, Huang R, Huang L-Y, Marcink T, et al. Structure of an endosomal signaling GPCR–G protein–β-arrestin megacomplex. Nat Struct Mol Biol. 2019 Dec;26(12):1123–31. [PubMed: 31740855]
66. Huang W, Masureel M, Qu Q, Janetzko J, Inoue A, Kato HE, et al. Structure of the neurotensin receptor 1 in complex with β-arrestin 1. Nature. 2020 Mar 12;579(7798):303–8. [PubMed: 31945771]
67. Park JY, Qu C, Yun MW, Yang F, He Q, Kim K, et al. Scaffolding mechanism of arrestin-2 in the cRaf/MEK1/ERK signaling cascade. PNAS. In press.
68. Vishnivetskiy SA, Zhan X, Chen Q, Iverson TM, Gurevich VV. Arrestin Expression in E. coli and Purification. Curr Protoc Pharmacol. 2014 Dec 1;67:2.11.1–2.11.19.
69. Otwinowski Z, Minor W. [20] Processing of X-ray diffraction data collected in oscillation mode. In: Methods in Enzymology [Internet]. Academic Press; 1997 [cited 2020 Nov 3]. p. 307–26. (Macromolecular Crystallography Part A; vol. 276). Available from: http://www.sciencedirect.com/science/article/pii/S007668799776066X
70. McCoy AJ, Grosse-Kunstleve RW, Adams PD, Winn MD, Storoni LC, Read RJ. Phaser crystallographic software. J Appl Crystallogr. 2007 01;40(Pt 4):658–74. [PubMed: 19461840]
71. Adams PD, Afonine PV, Bunkóczi G, Chen VB, Davis IW, Echols N, et al. PHENIX: a comprehensive Python-based system for macromolecular structure solution. Acta Crystallogr D Biol Crystallogr. 2010 Feb;66(Pt 2):213–21. [PubMed: 20124702]
72. Martín-García JM, Luque I, Mateo PL, Ruiz-Sanz J, Cámara-Artigas A. Crystallographic structure of the SH3 domain of the human c-Yes tyrosine kinase: Loop flexibility and amyloid aggregation. FEBS Letters. 2007;581(9):1701–6. [PubMed: 17418139]
73. Emsley P, Lohkamp B, Scott WG, Cowtan K. Features and development of Coot. Acta Crystallogr D Biol Crystallogr. 2010 Apr;66(Pt 4):486–501. [PubMed: 20383002]
74. Lee W, Tonelli M, Markley JL. NMRFAM-SPARKY: enhanced software for biomolecular NMR spectroscopy. Bioinformatics. 2015 Apr 15;31(8):1325–7. [PubMed: 25505092]

75. Molecular Operating Environment (MOE) 2013.08, Chemical Computing Group Inc: 1010 Sherbooke St. West, Suite #910, Montereal, QC, Canada, H3A 2R7.
76. Case DA, Cheatham TE, Darden T, Gohlke H, Luo R, Merz KM, et al. The Amber biomolecular simulation programs. Journal of Computational Chemistry. 2005;26(16):1668–88. [PubMed: 16200636]
77. Maier JA, Martinez C, Kasavajhala K, Wickstrom L, Hauser KE, Simmerling C. ff14SB: Improving the Accuracy of Protein Side Chain and Backbone Parameters from ff99SB. J Chem Theory Comput. 2015 Aug 11;11(8):3696–713. [PubMed: 26574453]
78. Price DJ, Brooks CL. A modified TIP3P water potential for simulation with Ewald summation. J Chem Phys. 2004 Nov 22;121(20):10096–103. [PubMed: 15549884]
79. Miyamoto S, Kollman PA. Settle: An analytical version of the SHAKE and RATTLE algorithm for rigid water models. Journal of Computational Chemistry. 1992;13(8):952–62.
80. Zwanzig R Nonlinear generalized Langevin equations. J Stat Phys. 1973 Nov 1;9(3):215–20.
81. Åqvist J, Wennerström P, Nervall M, Bjelic S, Brandsdal BO. Molecular dynamics simulations of water and biomolecules with a Monte Carlo constant pressure algorithm. Chemical Physics Letters. 2004 Jan 26;384(4):288–94.
82. Roe DR, Cheatham TE. PTRAJ and CPPTRAJ: Software for Processing and Analysis of Molecular Dynamics Trajectory Data. J Chem Theory Comput. 2013 Jul 9;9(7):3084–95. [PubMed: 26583988]
83. Alekseenko A, Ignatov M, Jones G, Sabitova M, Kozakov D. Protein-Protein and Protein-Peptide Docking with ClusPro Server. In: Protein Structure Prediction. 4th editon. 2020. p. 157–74. (Methods in Molecular Biology; vol. 2165).
84. Comeau SR, Gatchell DW, Vajda S, Camacho CJ. ClusPro: a fully automated algorithm for protein-protein docking. Nucleic Acids Research. 2004 Jul 1;32(Web Server):W96–9. [PubMed: 15215358]
85. Kozakov D, Hall DR, Xia B, Porter KA, Padhorny D, Yueh C, et al. The ClusPro web server for protein–protein docking. Nat Protoc. 2017 Feb;12(2):255–78. [PubMed: 28079879]
86. Molecular Operating Environment (MOE), C.C.G.U., 1010 Sherbrooke St. West, Suite#910, Montreal, QC, Canada, H3A 2R7. 2020.

HIGHLIGHTS

- Arrestins scaffold Fgr in a signal initiation complex
- A polyproline sequence in the aSwI region of arrestin-3 binds the Fgr SH3 domain
- Assays with arrestin-3 variants support this interaction in cells
- Patient mutations of the Fgr SH3 domain suggest this interaction occurs in humans
- A model of the signal initiation complex suggests a likely interaction mode

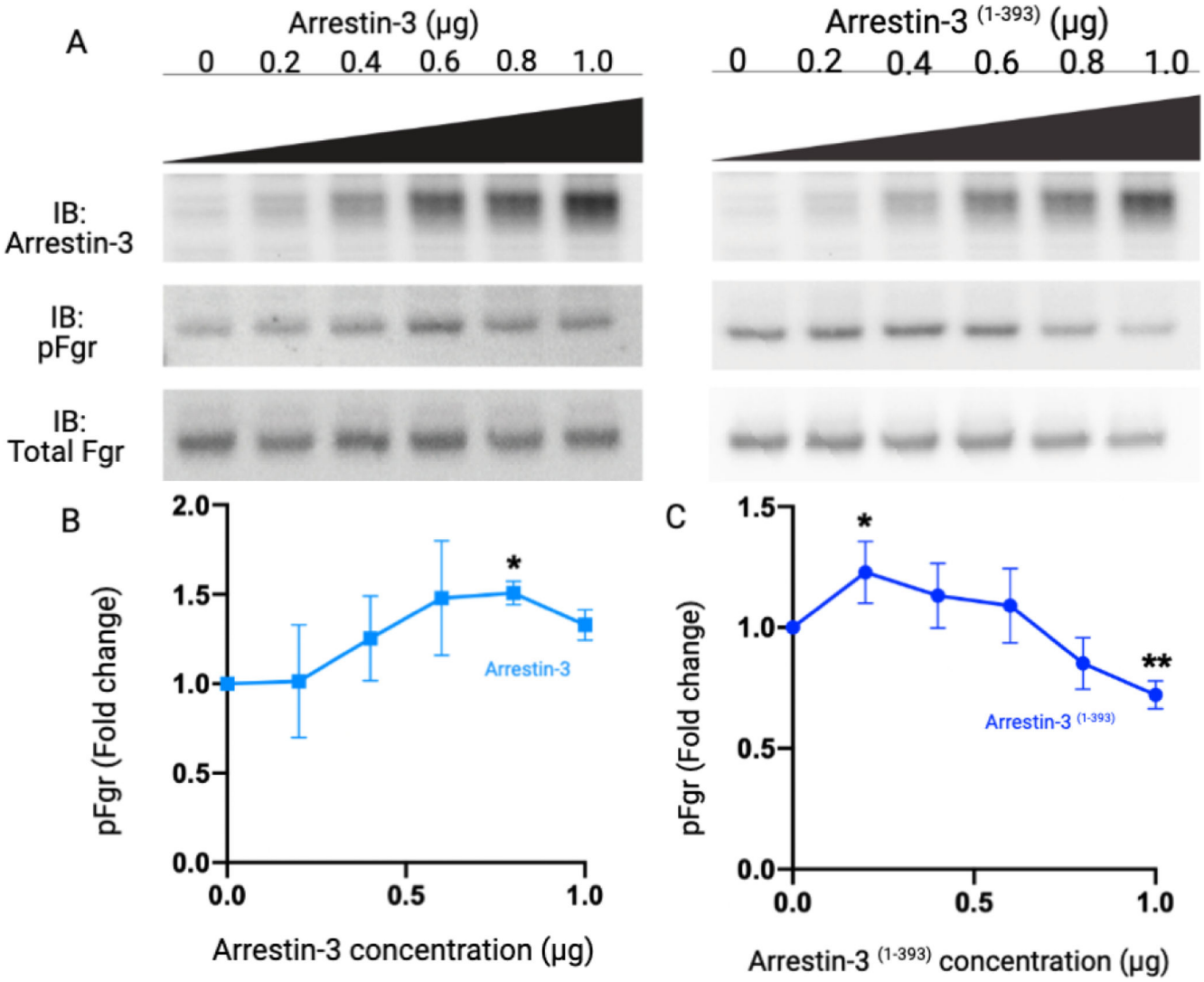

Figure 1. Arrestin-3-dependent Fgr phosphorylation exhibits bell-shaped concentration dependence.

Arrestin-2/3 knockout HEK293 cells (38) were co-transfected with Fgr kinase (0.05μg) and increasing amounts (0–1μg) of arrestin-3 (1–393). **(A)** Representative western blots of Fgr phosphorylation at Tyr-412 in the presence of full-length arrestin-3 and arrestin-3$^{(1–393)}$. **(B)** Dosimetric quantification of the westerns using Image Studio Lite software (LI-COR Biosciences). The intensity of phosphor-Fgr band was normalized to the intensity of the total Fgr band and shown as fold change in Fgr phosphorylation relative to cells without transfected arrestin-3. Statistical significance of the differences in pFgr was analyzed by one-way ANOVA followed by Dunnett's multiple comparison test. The pFgr level at each arrestin concentration was compared to the pFgr level with no arrestin present; (*$p < 0.05$; ANOVA summary: *$p = 0.0449$, $F_x = 3.22$, $R^2 = 0.5731$). Means ± SD from three independent experiments are shown. **(C)** Dosimetric quantification of the westerns using Image Studio Lite software (LI-COR Biosciences). The intensity of phospho-Fgr band was normalized to the intensity of the total Fgr band and shown as fold change in Fgr phosphorylation relative to cells without transfected arrestin-3. Statistical significance of

the differences in pFgr was analyzed by one-way ANOVA followed by Dunnett's multiple comparison test. The pFgr level at each arrestin concentration was compared to the pFgr level with no arrestin present; (*$p < 0.05$, **$p < 0.01$; ANOVA summary: ***$p < 0.0001$, $F_x = 10.66$, $R^2 = 0.6896$). The means ± SD from three independent experiments are shown.

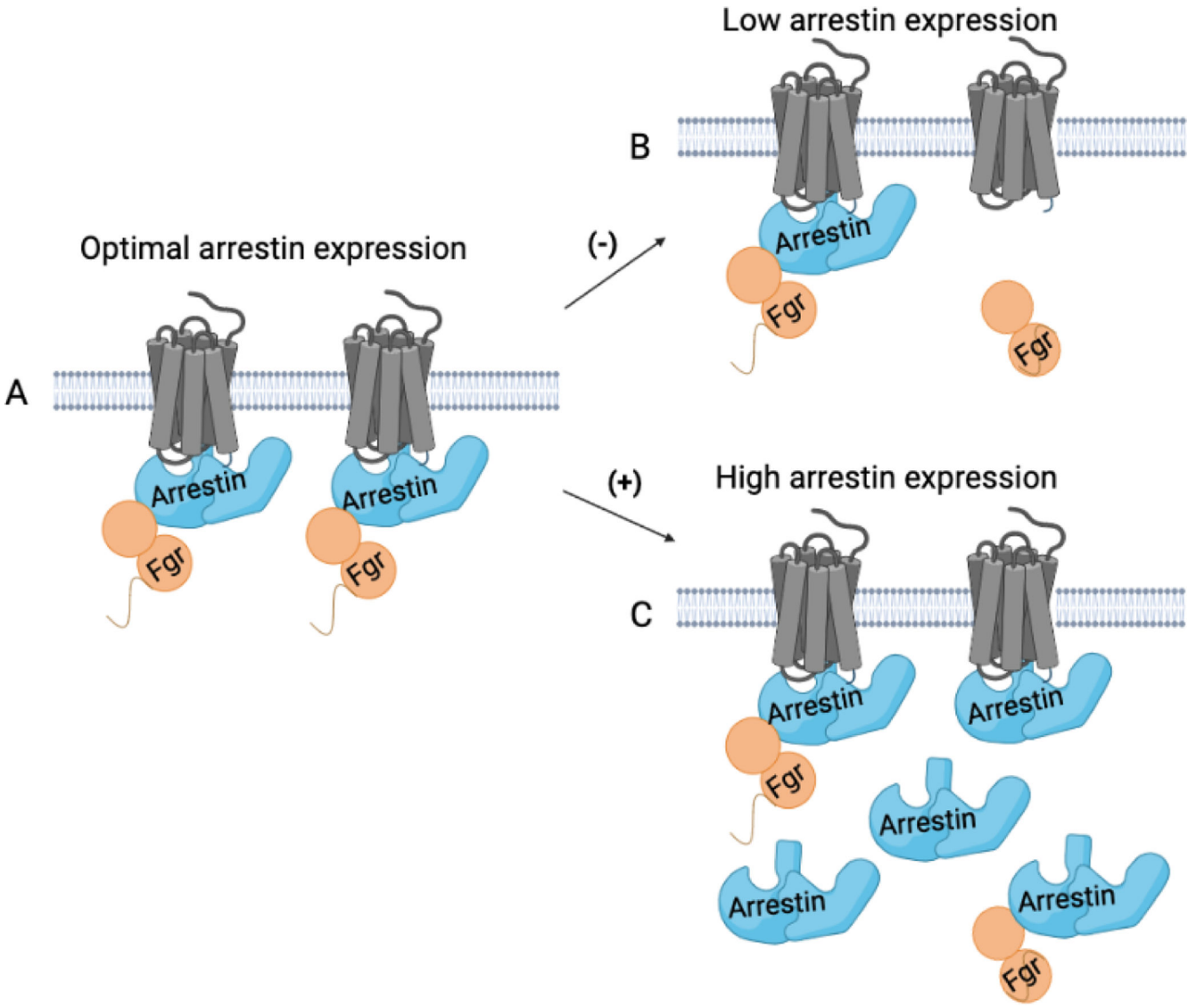

Figure 2. Effect of arrestin-3 concentration on the formation of functional signaling complexes of Fgr kinase during scaffolding.

A schematic representation of scaffolding of Fgr by arrestin-3 shows the effects of changing arrestin-3 concentration. The schematic assumes a 1:1 complex between arrestin-3 and the Fgr kinase. **(A)** Under equimolar conditions, arrestin-3 bridges receptor and Fgr kinase in functional complexes. **(B)** At low arrestin-3 expression, fewer functional signaling complexes are formed due to insufficient amounts of arrestin-3. **(C)** At excess of arrestin-3 over Fgr and receptors Fgr may bind to arrestins that are not receptor associated; thus, despite increased availability of arrestin-3, fewer functional signaling complexes are formed than in panel (**A**). Figure was made using BioRender (Biorender.com).

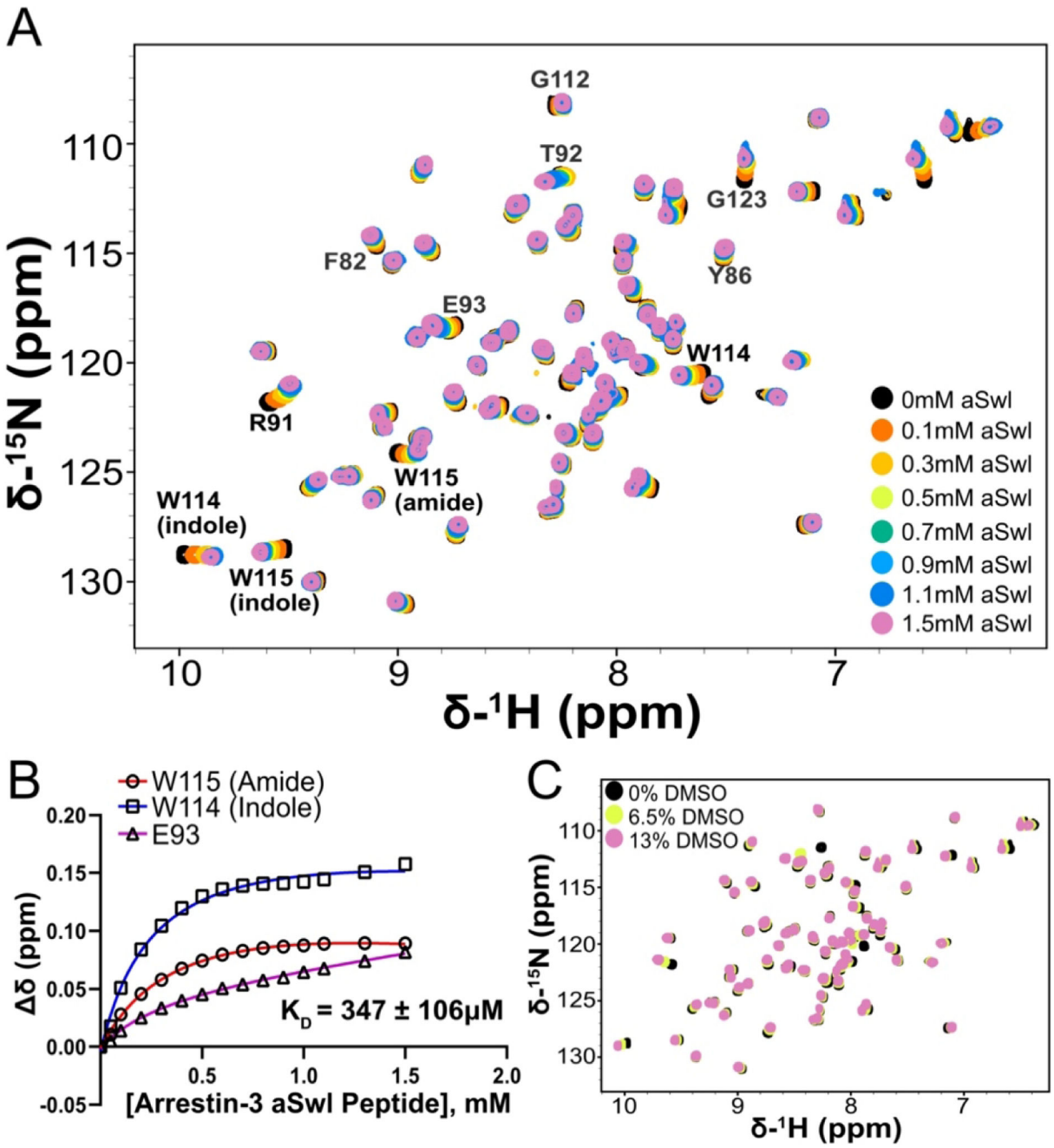

Figure 3. The Fgr SH3 interacts with the polyproline motif of arrestin-3.

(A) Representative spectra of the titration of Fgr SH3 domain with arrestin-3 aSwI peptide (**PP**T**P**N**PP**R**PP**). This titration was performed once and fit using a total binding K_D model. Error was determined as the error of the fit for the curve. **(B)** Representative dose-response curves for indicated resonances. **(C)** Buffer controls, containing increasing amounts of DMSO matching DMSO in peptide titrations. Data shown here are n=1, and error was propagated using the square sum of the respective errors of the fit.

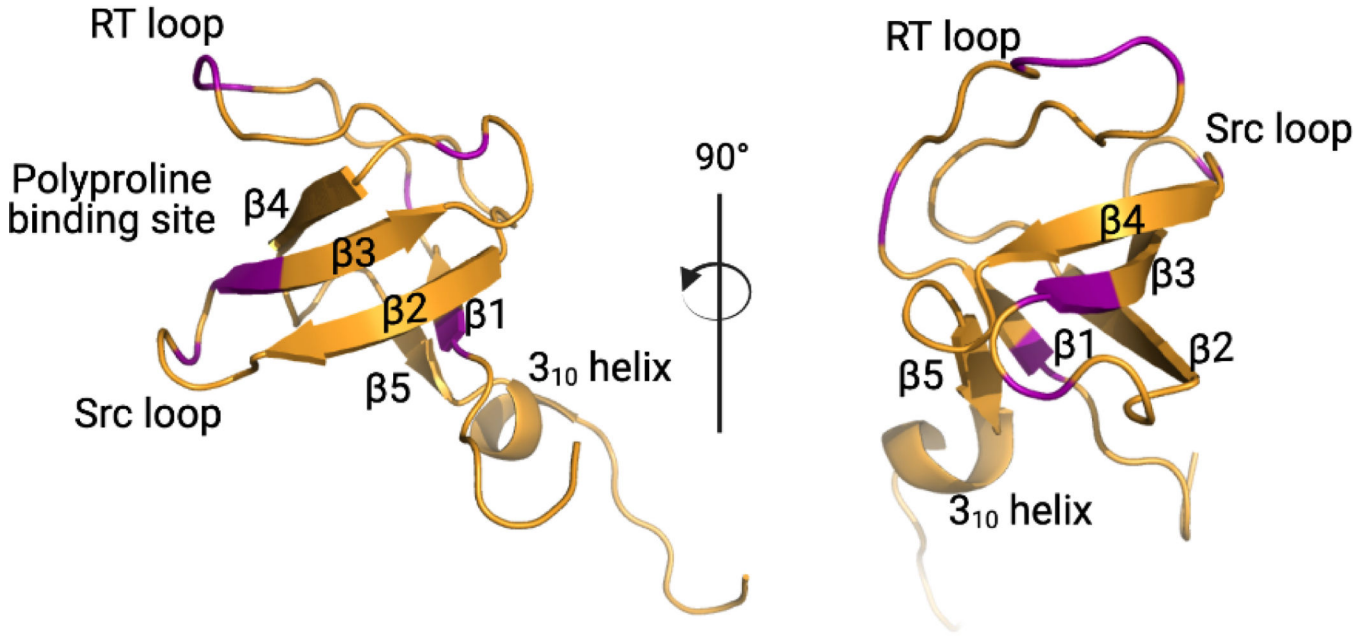

Figure 4. Crystal structure of the SH3 domain of Fgr at 1.9 Å resolution.

Ribbon representation of the crystal structure of the Fg SH3 domain. The structure contains all features of a canonical SH3 domain. These are five anti-parallel β-strands (β1– β5), the RT loop, the n-Src loop, the distal loop, and a short 3_{10} helix located near the C-terminus. NMR responsive sites are shown in purple. Figure was made using BioRender (Biorender.com).

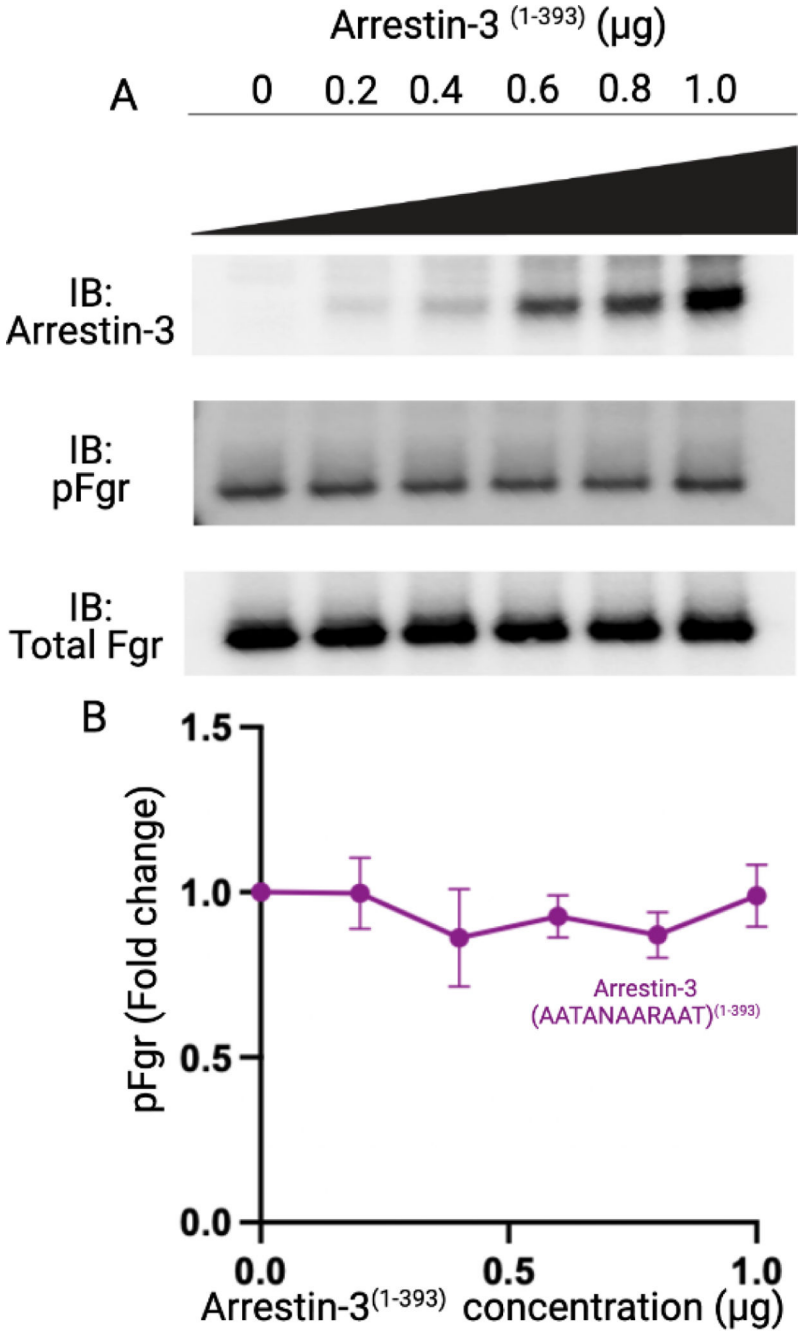

Figure 5. Effect of the arrestin-3 aSwI polyproline sequence on Fgr kinase activation.

Arrestin-2/3 knockout HEK293 cells were co-transfected with Fgr kinase and 0–1 μg of arrestin-3$^{(1–393)}$ with the prolines within the aSwI replaced with alanines (**AA**T**A**N**AA**R**AA**T). **(A)** Representative western blots showing that Fgr phosphorylation did not change upon transfection with the arrestin-3-(**AA**T**A**N**AA**R**AA**T)$^{(1–393)}$ mutant. **(B)** Quantification using Image Studio Lite software (LI-COR Biosciences) shown as fold change in Fgr phosphorylation. The intensity of phospho-Fgr band was normalized to the intensity of the total Fgr band and shown as fold change in Fgr phosphorylation relative to cells without transfected arrestin-3. Statistical significance of the differences in pFgr

levels in the presence of arrestin-3-$(AATANAARAAT)^{(1–393)}$ was analyzed by one-way ANOVA followed by Dunnett's multiple comparison test. The pFgr level at each arrestin concentration was compared to the pFgr level with no arrestin. No statistically significant differences were detected (ANOVA summary: $p = 0.27981$, $F_x = 1.438$, $R^2 = 0.3748$). Means ± SD from three independent experiments are shown.

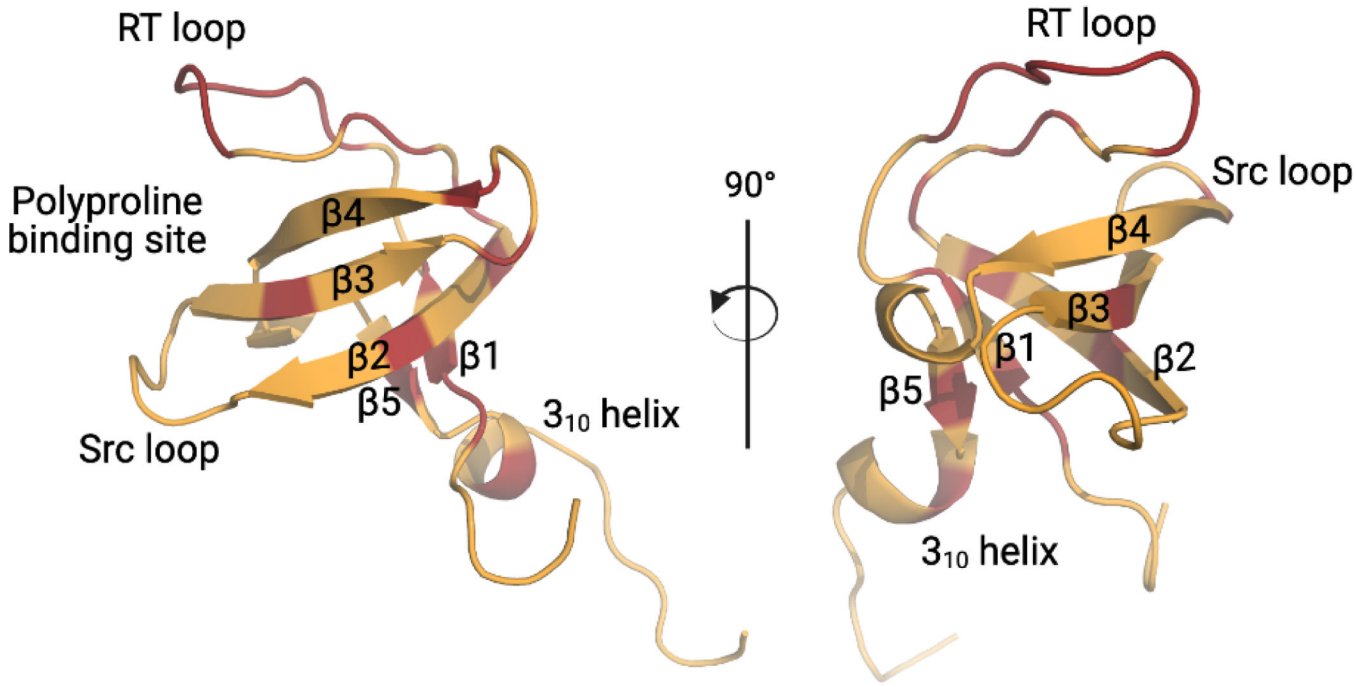

Figure 6. Location of cancer-associated mutations on the Fgr SH3 domain.

Cancer-associated single-point mutations are mapped onto the crystal structure of the Fgr SH3 domain in red. Figure was made using BioRender (Biorender.com).

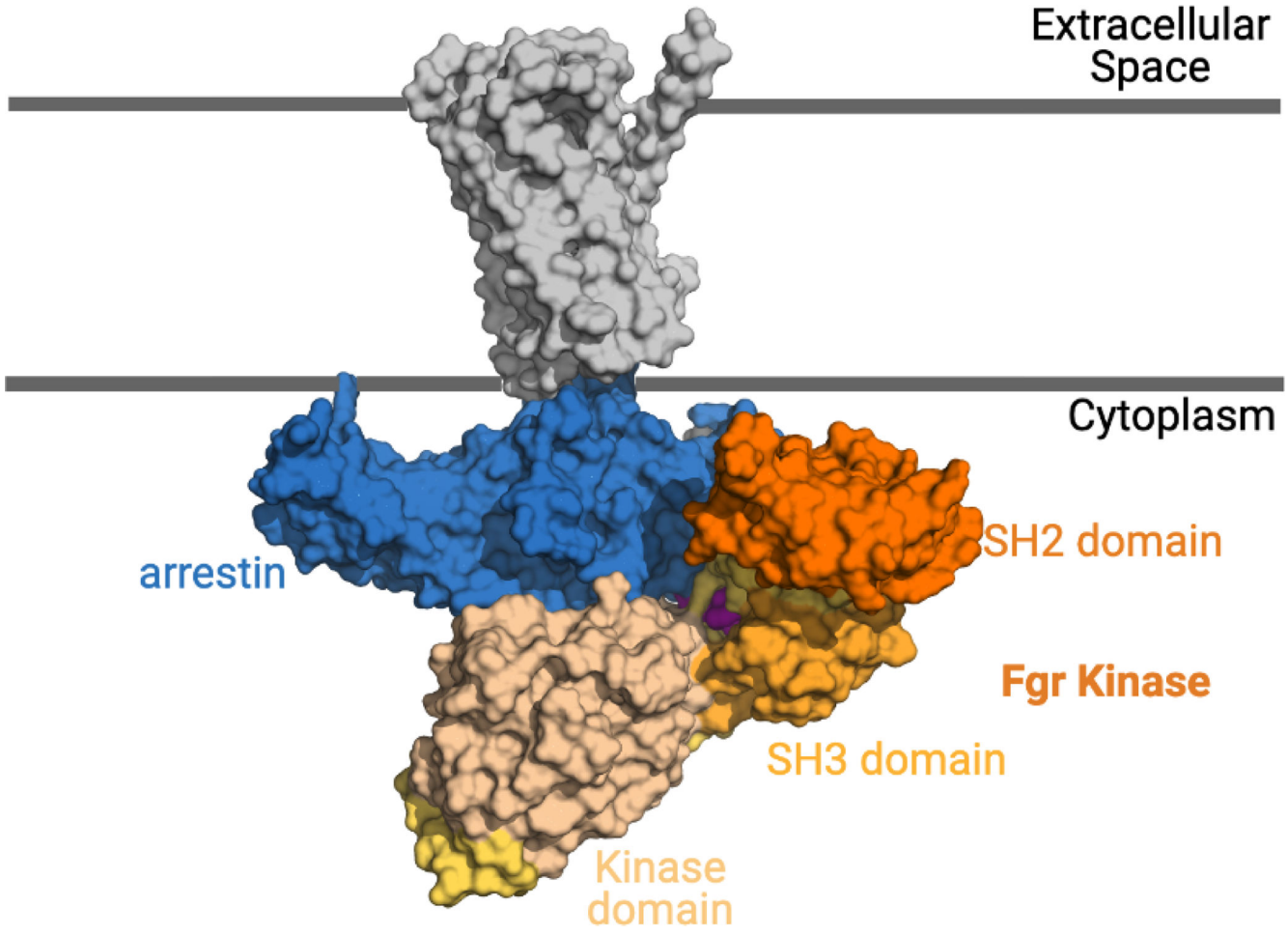

Figure 7. Model of a GPCR-arrestin-3-Fgr signal initiation complex.

Model of interaction between active G protein-coupled receptor (gray) with active arrestin-3 (blue) bound to Fgr kinase (orange). In this model, the SH3 domain (light orange) interacts with arrestin-3 via the polyproline motif (magenta). The SH2 domain (bright orange) and the kinase domain (wheat) also interact with activated arrestin-3. The C-lobe of arrestin-3 and the SH2 domain of Fgr kinase may interact with the membrane. Figure was made using BioRender (Biorender.com).

Table 1.
Summary of crystallographic data collection and refinement statistics.

Values in parentheses are for the highest resolution shell, 1.96 – 1.93 Å resolution.

Data collection statistics	
Beamline	SSRL Beamline BL9-2
Wavelength	0.97946 Å
Resolution	31.5–1.93 Å (1.96–1.93 Å)
Space group	I 2 2 2
Unit-cell dimensions	a=35.55 Å b=53.29 Å c=67.48 Å
R_{sym}	0.092 (0.468)
I/σ	15.9 (2.56)
Completeness (%)	97.5 (93.9)
Redundancy	4.6
$CC_{1/2}$	1 (0.778)
Refinement Statistics	
PDB entry	7JT9
Number of Reflections	4945
Unique reflections	4945
R_{cryst}	0.186
R_{free}	0.217
RMSD bond lengths	0.005
RMSD bond angles	0.73
Ramachandran	
Favored	99 %
Additionally allowed	1%
Disallowed	0%

Table 2.
Cancer-associated mutations in the Fgr SH3 domain.

The table summarizes the cancer-associated mutations, type of cancer associated with each mutation, and the location of the mutation on the Fgr SH3 domain.

Fgr SH3 Cancer Mutations

Mutation	Cancer	Location
L81R	Melanoma	N-terminus
F82S	Lung cancer	N-terminus
A84V	Uterine cancer	β1 strand
Y88C	Melanoma	RT loop
E89K	Cervical cancer	RT loop
A90T	Uterine cancer	RT loop
R91Q	Melanoma	RT loop
T92N	Blastoma, Liver cancer	RT loop
E93A	Lung cancer	RT loop
D94N	Bone cancer	RT loop
T97S	Head and neck cancer	RT loop
F98L	Liver cancer	RT loop
K100N	Uterine cancer	RT loop
E102D, E102V	Uterine cancer, Stomach cancer	RT loop
H105R, H105Q	Urinary bladder cancer, Liver cancer	β2 strand
E116K	Melanoma, Urinary bladder cancer	β3 strand
L120V	Urinary bladder cancer	Distal loop
G123E	Thyroid carcinoma	Distal loop
A134D	Prostate cancer	β5 strand
D137A	Pancreatic cancer	3_{10} helix